18. S. Levitus, *J. Geophys. Res. Oceans*, **94**, 6091 (1989).
19. J. Hansen *et al.*, *J. Geophys. Res.* **102**, 25679 (1997).
20. K. Hasselmann, R. Sausen, E. Maier-Reimer, R. Voss, *Clim. Dyn.* **9**, 53 (1993).
21. J. Hansen *et al.*, *J. Geophys. Res.* **93**, 9341 (1988).
22. J. R. N. Lazier, in *Natural Climate Variability on Decade-to-Century Time Scales*, D. G. Martinson *et al.*, Eds. (National Academy Press, Washington, DC, 1995), chap. 3, pp. 295–302.
23. R. Dickson, J. Lazier, J. Meincke, P. Rhines, J. Swift, *Prog. Oceanogr.* **38**, 241 (1996).
24. S. Nerem, D. P. Chambers, E. W. Leuliette, G. T. Mitchum, B. S. Giese, *Geophys. Res. Lett.* **26**, 3005 (1999).
25. R. W. Reynolds and T. S. Smith, *J. Clim.* 7, 929 (1994).
26. D. W. J. Thompson and J. M. Wallace, *Geophys. Res. Lett.* **25**, 1297 (1998).
27. D. T. Shindell *et al.*, *Nature*, **399**, 452 (1999).
28. J. Perlwitz and H.-F. Graf, *J. Clim.* **8**, 2281 (1995).
29. A. Kitoh *et al.*, *Geophys. Res. Lett.* **23**, 543 (1996).
30. M. P. Baldwin *et al.*, *Geophys. Res. Lett.* **21**, 1141 (1994).
31. X. Cheng and T. J. Dunkerton, *J. Clim.* **8**, 2631 (1995).
32. The construction of the analyses shown in this work was supported by grants from the NOAA Climate and Global Change program. Preparation of the databases used in this work was supported by the NOAA and NOAA/NASA Climate and Global Change programs and the NOAA ESDIM program. J.I.A. is a University Corporation for Atmospheric Research (UCAR) Project Scientist at NODC/NOAA.

8 November 1999; accepted 11 February 2000

A *Drosophila* Mechanosensory Transduction Channel

Richard G. Walker,[1] Aarron T. Willingham,[1] Charles S. Zuker[2]*

Mechanosensory transduction underlies a wide range of senses, including proprioception, touch, balance, and hearing. The pivotal element of these senses is a mechanically gated ion channel that transduces sound, pressure, or movement into changes in excitability of specialized sensory cells. Despite the prevalence of mechanosensory systems, little is known about the molecular nature of the transduction channels. To identify such a channel, we analyzed *Drosophila melanogaster* mechanoreceptive mutants for defects in mechanosensory physiology. Loss-of-function mutations in the *no mechanoreceptor potential C* (*nompC*) gene virtually abolished mechanosensory signaling. *nompC* encodes a new ion channel that is essential for mechanosensory transduction. As expected for a transduction channel, *D. melanogaster* NOMPC and a *Caenorhabditis elegans* homolog were selectively expressed in mechanosensory organs.

Our capacity to hear a whisper across a crowded room, detect our position in space, and coordinate our limbs during a stroll through the park is conferred by the mechanical senses. Mechanosensory transduction is the process that converts mechanical forces into electrical signals. When mechanoreceptors are stimulated, mechanically sensitive cation channels open and produce an inward transduction current that depolarizes the cell. The opening of mechanosensory transduction channels in vertebrate hair cells takes place within a few microseconds after the onset of a stimulus, too quickly for the generation of second messengers (*1*). Mechanical stimuli are therefore hypothesized to directly gate these channels. This mode of activation is in sharp contrast to other sensory modalities, such as vision, olfaction, and taste, which use stereotypical G protein–coupled cascades to modulate transduction channels.

Most models of mechanosensory signaling propose that transduction channels be anchored on both sides of the membrane, so that relative movements between the extracellular matrix and the cytoskeleton produce the mechanical tension that gates these channels. In the gating-spring model of mechanosensory transduction in vertebrate hair cells (*2, 3*), deflection of the mechanically sensitive hair bundle produces shear between adjacent stereocilia that stretches the gating springs. This increase in tension "pulls" the transduction channels open, depolarizes the cell, and triggers neurotransmitter release. Although biophysical data support this model for transduction in hair cells, the molecular identity of the mechanically gated ion channel remains unknown. This is largely due to the paucity of sensory tissue and the small number of transduction channels in each hair cell (*4*).

Genetic approaches are ideally suited for identifying rare molecules involved in mechanosensory transduction (*5–10*). The isolation of genetic mutations does not depend on any assumptions about the nature or abundance of the target molecules, other than loss of their function results in a recognizable phenotype. The most extensive genetic dissection of mechanosensory behavior was based on screens for *Caenorhabditis elegans* touch-insensitive mutants. These studies identified genes involved in the development, survival, function, and regulation of touch receptor neurons (*11*). Of particular interest were those that likely function in the mechanoelectrical transduction process. This group included degenerins, collagen, stomatin, and tubulins, a finding consistent with the expectation that mechanosensory signaling involves finely orchestrated interactions between ion channels, extracellular matrix, and cytoskeletal components (*12*).

Degenerins (MEC-4, MEC-10, DEG-1, UNC-8, and UNC-105) are a family of *C. elegans* ion channels related to vertebrate epithelial sodium channels (*13*). Because of their critical role in the touch receptor neurons, degenerins have been proposed to function as mechanosensory transduction channels (*13*). More recently, a *C. elegans* transient receptor potential (TRP) family member, OSM-9, was shown to be involved in mechanotransduction because it is expressed in sensory dendrites of a subset of ciliated sensory neurons and is required for osmosensation and nose touch (*14*). Although these genetic studies demonstrated the requirement for degenerins and OSM-9 in mechanoreception, there are no electrophysiological data supporting a role for these channels in the actual transduction process.

Drosophila is an attractive model to dissect mechanosensation because it is possible to combine genetic manipulations with electrophysiological recordings from mechanoreceptor neurons (*7*). The fly's mechanosensory repertoire includes touch, proprioception, and hearing, mediated by the complement of sensory bristles, campaniform sensilla, chordotonal organs, and type II mechanoreceptors (*15*). Of these, sensory bristles are particularly amenable to physiological manipulation in the intact animal. Each mechanosensory bristle organ is composed of a hollow hair shaft whose base impinges on the dendritic tip of a bipolar sensory neuron (Fig. 1A). The shaft thus acts as a tiny lever arm in which deflections of the external bristle compress the neuron's dendritic tip and gate the transduction channels (*16*). The mechanosensory dendrite is bathed in an unusual high-K^+, low-Ca^{2+} fluid (*17*), which provides a large positive driving force into the neuron; opening of transduction channels depolarizes the cell and promotes neurotransmitter release.

To identify components of the mechanotransduction machinery, we screened *Drosophila* touch-insensitive and proprioceptive mutants (*7*) for defects in the physiology of mechanosensory responses. Those mutants that most likely defined transduction molecules were then characterized.

Wild-type mechanosensory response. To gain electrical access to the sensory neuron,

[1]Departments of Biology and Neurosciences and [2]Howard Hughes Medical Institute, University of California, San Diego, La Jolla, CA 92093–0649, USA.

*To whom correspondence should be addressed. E-mail: charles@flyeye.ucsd.edu

we removed the tip of the hollow sensory bristle, placed a recording/stimulation pipette over its end, and delivered calibrated mechanical stimuli while recording transduction currents with a voltage-clamp apparatus (*17, 18*). We analyzed responses from wild-type *Drosophila*, focusing on electrophysiological features that characterize vertebrate mechanosensory transduction systems: directional sensitivity, steep displacement-response relations, submillisecond latencies between stimulus and response, and sensitivity to displacements of only a few angstroms (*3, 4*).

Asymmetries in the ultrastructure and transduction machinery of vertebrate mechanosensory organs endow them with directional sensitivity. We reasoned that similar asymmetries may confer directional selectivity to fly bristles (*19*). Mechanoreceptor currents (MRCs) were recorded from macrochaete bristles throughout the thorax, and all displayed strong directional sensitivity. For instance, when an anterior notopleural bristle was deflected toward the surface of the body, it generated a robust response (Fig. 1B). In contrast, stimuli in all other directions elicited minimal transduction currents. Hereafter, stimuli in the excitatory direction will be referred to as "positive," and those in the opposite direction will be referred to as "negative."

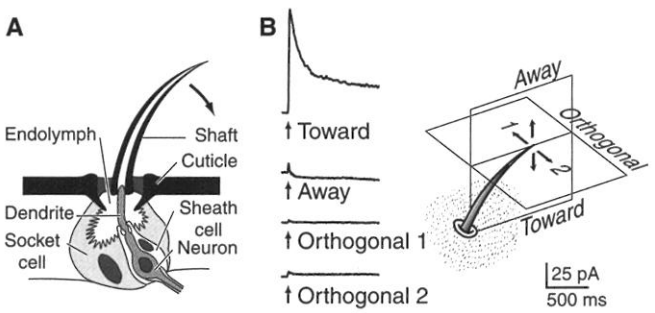

Fig. 1. (**A**) Diagram of a *Drosophila* mechanoreceptor bristle. The bristle sensory organ is composed of a hollow hair shaft and three cells: the socket cell, the sheath cell, and a ciliated mechanosensory neuron (*19*). The dendritic tip resides in an unusual high-K^+ endolymph, which creates a TEP of +40 mV, which in turn provides a large (~120-mV) driving voltage into the neuron. Displacement of the shaft compresses the dendritic tip and opens the transduction channels. Clipping the hair shaft and placing a recording electrode over the tip allows electrical access to the underlying neuron. (**B**) Directional sensitivity of a ventral notopleural bristle. Step stimuli of 20 μm were applied in each of four directions: toward and away from the body of the fly and in the two orthogonal directions depicted. Displacements toward the body of the fly elicited a robust 100-pA transient current, whereas stimuli away from the fly or in the orthogonal directions produced responses of only a few pA. The decrease below the resting current level during the away stimulus probably reflects a closure of the small number of channels open at rest.

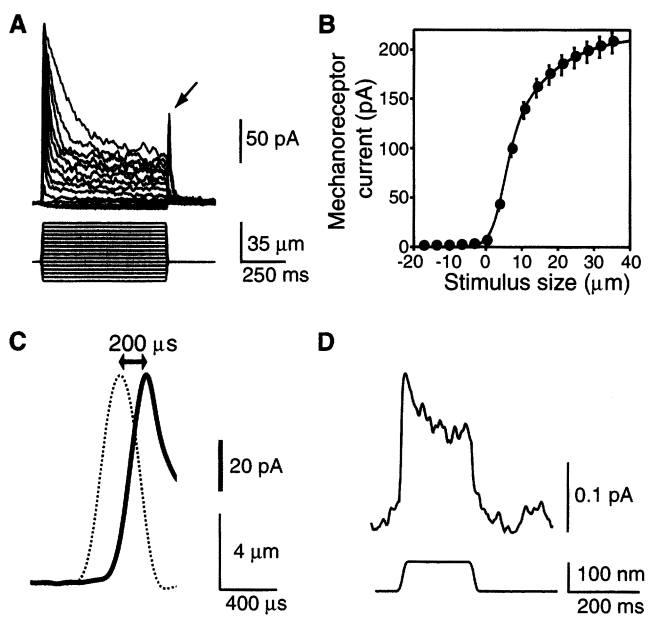

Fig. 2. Voltage-clamp characterization of wild-type mechanosensory currents. (**A**) A family of 15 step displacements that ranged between −17.5 and +35 μm (lower traces) were delivered to a bristle while transduction currents were recorded (upper traces). The TEP was clamped at +40 mV during each 700-ms stimulus (*18*). For saturating positive displacements, the transduction currents peaked at ~210 pA. During negative displacements, the current slowly declined to about −6 pA. When the bristle was returned to its resting position, the neuron generated a robust response (indicated by arrow). This reflects adaptation. Each trace represents the average of five responses. (**B**) The graph shows a plot of MRCs versus stimulus size. Shown are averages of 20 experiments (error bars, ±SEM). The line through the points represents a best fit with a three-state model used to describe hair-cell transduction (*20*). The MRC saturated at displacements of ~35 μm, with maximum sensitivity occurring between 0 and +10 μm. (**C**) The latency of the response was measured by applying a 10-μm stimulus (dotted trace) while measuring the MRC (6-μs sampling interval and 10-kHz cutoff frequency). The bold trace shows the average response to 15 stimuli; this response trailed the stimulus with a 200-μs delay. (**D**) Bristle mechanoreceptors are sensitive to nanometer deflections. A 100-nm step stimulus, which represents a deflection of ~2 nm at the base of a 100-μm bristle, elicited a 0.2-pA transduction current. Because a response of this size would normally be lost in the 0.5- to 2-pA noise floor, we averaged responses to 100 stimuli.

To characterize the range of responses of a macrochaete, we gave sensory bristles positive and negative step stimuli that ranged between +35 and −17.5 μm (Fig. 2A, lower traces). During positive displacements, we recorded a transient increase in the MRC that peaked at ~210 pA and was followed by a gradual, but incomplete, decline to the resting current level (Fig. 2A, upper traces). During negative displacements, only a small negative MRC was observed (−6 pA). Because the neuron adapted to this new negative position, the return of the bristle to its resting state is sensed as a positive deflection and results in a concomitant 100-pA transient current. A displacement-response curve derived from 20 thoracic bristles was fitted using a three-state model (*20*); the results showed that the mechanoreceptor neuron is most sensitive to stimuli between 0 and 10 μm and saturates at ~35 μm (Fig. 2B).

Recording of fly mechanoreceptor responses under conditions that allow the detection of microsecond-scale events showed latencies of ~200 μs (Fig. 2C). Because this response time is ~100 times as fast as the fastest known second-messenger cascade, fly mechanosensory transduction is unlikely to rely on second messengers.

Vertebrate hair cells detect mechanical stimuli of atomic dimensions (*4*). Although we were unable to deliver displacements this small, we elicited small transduction currents by stimuli of only 100 nm (Fig. 2D). Because of the lever action of the bristle shaft, however, a 100-nm stimulus at the end of a cut bristle produces a much smaller displacement at the neuronal dendritic tip. On the basis of the geometry of the fly macrochaete bristles (*21*), we estimate that the corresponding displacement at the base of the bristle would be ~50-fold less, or 2 nm. This level of sensitivity would allow the neuron to perceive displacements of only one-half the thickness of its plasma membrane.

Adaptation permits mechanoreceptors to continuously adjust their range of responsiveness, thus enabling the cell to detect new displacements in the presence of an existing stimulus. In vertebrate hair cells, the adaptation machinery restores nearly the full dynamic range of response with each maintained displacement (*22*). To investigate adaptation in fly mechanoreceptors, we measured the response to a series of test stimuli before and during adapting steps that varied between −14 and +14 μm (Fig. 3A). Responses obtained before the adapting steps were then used to produce an $I(X)$ curve that was shifted along the displace-

ment axis to fit the data generated during each adapting stimulus (Fig. 3B) (*22*). By plotting the size of the shift as a function of the size of the adapting step, we measured how much of the cell's response is retained at each adapting step. The adaptation process preserved ~85% of the dynamic range (slope = 0.85; Fig. 3C). Incomplete adaptation may allow the cell to continue to "perceive" the sustained stimulus yet remain receptive to new stimuli. This level of adaptation closely resembles that seen in vertebrate hair cells (*22*); the similarity also extended to the time course (time constant = 18 ms) of the adaptation process (Fig. 3D) (*22*). Together, these results suggest that the core transduction components in fly bristles and vertebrate hair cells are functionally related.

***nompC* mechanosensory responses.** To identify components of the transduction machinery, we screened 27 different *Drosophila* mechanosensory transduction mutants (*7*) for defects in transduction currents. On the basis of uncoordinated phenotypes, these mutants fell into 20 complementation groups (*23*). One of these, *nompC*, was particularly interesting. At a behavioral level, three of the *nompC* alleles showed severe uncoordination, whereas another ($nompC^4$) showed moderate clumsiness. The three severe mutants ($nompC^1$, $nompC^2$, and $nompC^3$) displayed a dramatic loss of MRC, with transduction currents of ~10% that of control animals (Fig. 4, A and B). In contrast, the $nompC^4$ allele exhibited almost normal MRC amplitudes but displayed severely defective adaptation. The time constant of adaptation in $nompC^4$ was 50 ms, versus 277 ms for control flies (Fig. 4C). Because the MRC and the adaptation process are intimately tied to the function and regulation of the mechanically gated ion channel, we suspected that the *nompC* gene product was either a component of the adaptation machinery or a transduction channel.

Why are $nompC^4$ flies behaviorally uncoordinated, given that they have normal response amplitudes? One possibility is that the abnormally fast decay of the MRP would decrease the number of action potentials by limiting the

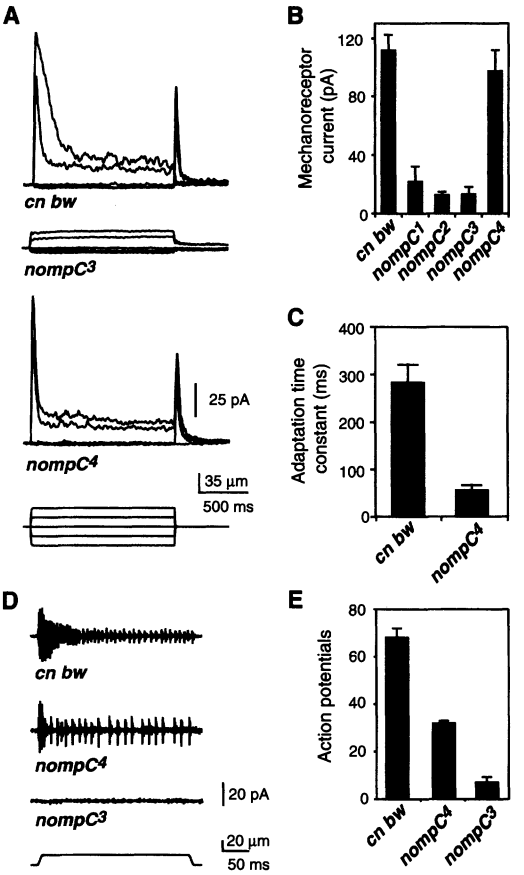

Fig. 4. Characterization of *nompC* transduction currents. (**A**) Responses of *nompC* mutants and control flies to a family of four displacements (lower traces). The control *cn bw* flies exhibited a robust current to a 35-μm step. $nompC^3$ and the two other severe *nompC* alleles showed a dramatic loss of MRC. $nompC^4$ showed a near-normal peak response but adapted noticeably faster than controls. (**B**) Quantitation of *nompC* mutant responses. The MRCs from a minimum of eight bristles were measured for each *nompC* allele. Peak MRCs were as follows: *cn bw* = 111 ± 11 pA [mean ± SEM (error bars) for 18 bristles], $nompC^1$ = 22 ± 10 pA (8 bristles), $nompC^2$ = 13 ± 2 pA (11 bristles), $nompC^3$ = 13 ± 5 pA (13 bristles), and $nompC^4$ = 97 ± 15 pA (15 bristles). (**C**) Adaptation time constants of $nompC^4$ mutants. Adaptation time constants were derived by fitting single-exponential curves to current traces from 35-μm steps (see Fig. 3D). The adaptation time constant for *cn bw* control flies (277 ± 37 ms, 18 bristles) is about five times as large as that of $nompC^4$ (50 ± 11 ms, 15 bristles). Error bars, ±SEM. (**D**) Action potentials were recorded during a single 20-μm step displacement of control and *nompC* mutant bristles. $nompC^3$ mutants have a near-complete loss of signaling, whereas $nompC^4$ mechanoreceptor neurons have a dramatic reduction in the frequency of action potentials. (**E**) The number of action potentials in *nompC* mutants during a 300-ms stimulus of 20 μm was as follows: *cn bw* = 68 ± 4 (15 bristles), $nompC^3$ = 7 ± 2 (3 bristles), and $nompC^4$ = 32 ± 1 (13 bristles). Error bars, ±SEM.

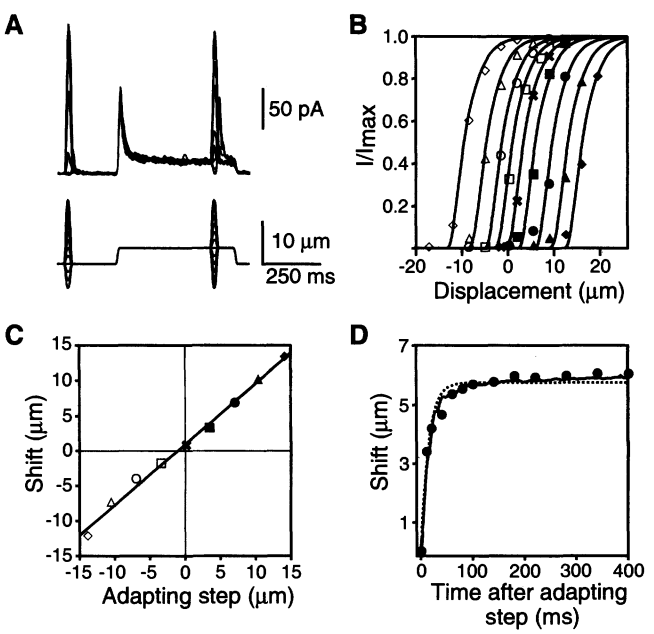

Fig. 3. Adaptation of fly mechanosensory transduction currents. (**A**) The adaptation state of a mechanosensory neuron was determined by giving a series of rapid test stimuli before and during a 500-ms adapting step. Bristles were given 12 test stimuli that ranged between −17.5 and +19.25 μm in 1.75-μm steps (lower traces). The upper traces in (A) show responses to a +3.5-μm adapting step. (**B**) Shift of displacement-response relations during adaptation (I_{max} = peak MRC). An $I(X)$ plot for test stimuli given before any adapting steps (crosses) was fitted with a curve from a three-state model (*20*). This curve was shifted along the abscissa to best fit $I(X)$ plots from adapting steps of 3.5 μm (squares), 7 μm (circles), 10.5 μm (triangles), and 14 μm (diamonds). Positive stimuli are shown as solid symbols, and negative stimuli are shown as open symbols. The data for each $I(X)$ curve were derived from three to five experiments. To clearly show the curves, the figure displays only half of the data points. (**C**) Extent of the adaptive shift. The size of each $I(X)$ curve shift was plotted against the size of its adapting step. The slope of this function (0.85) reflects the extent of the adaptive response. Symbols are as in (B). (**D**) Time course of the adaptive shift. Test stimuli like those shown in (A) were given before (time t = 0) and at 10, 20, 40, 60, 80, 100, 140, 180, 220, 280, 340, and 400 ms after the onset of a 7-μm adapting step. $I(X)$ relations were generated from each set of responses and fitted with a three-state relation as in (B). The function at t = 0 was shifted along the x axis to best fit the data from each time. The size of the shift is plotted versus the time after the onset of the 7-μm displacement (dots). These data were fitted with an exponential curve (dotted line), whose time constant was 18 ms. To illustrate that the transduction current accurately reflects the adaptation state of the cell, we inverted, scaled, and superimposed a current trace on the exponential curve (solid line).

time in which the cell is depolarized. To test this postulate, we stimulated control and *nompC*^{4} animals with a step stimulus while recording action potentials through the bristle (*17*). As hypothesized, the number of action potentials in *nompC*^{4} was less than half that of control flies (Fig. 4, D and E). These results explain the behavioral phenotype of *nompC*^{4} and further support *nompC* as a critical player in the transduction process.

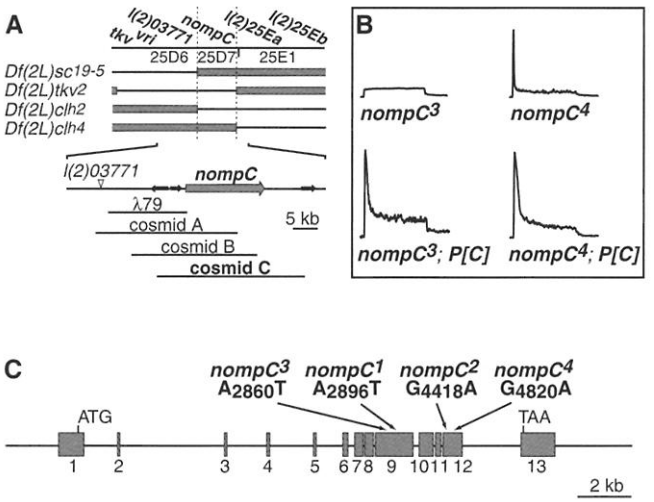

Fig. 5. Identification of the *nompC* gene. (**A**) Genetic and molecular characterization of the *nompC* interval. *nompC* was localized to the 25D7 region of the second chromosome by deficiency mapping. *Df(2L)tkv*^{2} and *Df(2L)cl*^{h2} deleted or disrupted *nompC*; *Df(2L)sc*$^{19\text{-}5}$ and *Df(2L)cl*^{h4} complemented the *nompC* phenotype; *l(2)25Dc* failed to complement *nompC* (deleted segments are indicated by thin lines). A phage clone (λ79) from a nearby chromosomal walk (*39*) was used as a starting point for isolating cosmids A through C (*24*). Arrows depict the orientation of predicted transcriptional units from cosmid C. (**B**) Cosmid C rescued the physiological and behavioral defects of all *nompC* alleles. (**C**) The diagram shows the structure of the *nompC* locus. The gene is divided into 13 exons, producing a 6.1-kb transcript. The structure was derived by comparison of genomic and cDNA sequences. ATG and TAA refer to the initiator and terminator codons, respectively. The location and nature of the mutations in the four *nompC* alleles are shown above the gene map.

Mapping, rescue, and cloning of *nompC*. *nompC* was mapped to position 25D7 on the left arm of the second chromosome (Fig. 5A). Three overlapping cosmid clones spanning this interval (Fig. 5A) were tested for rescue of the *nompC* phenotype by P element–mediated germ line transformation (*24*). Cosmid C fully rescued the physiological and behavioral defects of *nompC* mutants (Fig. 5B). Sequences from cosmid C were used to screen a *Drosophila* antennal cDNA library (*25*), and two 6.1-kb cDNAs were isolated. Sequence analysis of the full 33-kb cosmid and the two cDNA clones showed a single transcriptional unit encoding a predicted polypeptide of 1619 amino acids (Fig. 5C). This gene is split into 13 exons, spanning ~18 kb of genomic DNA. Using the polymerase chain reaction (PCR), we isolated this candidate gene from *nompC*^{1}, *nompC*^{2}, *nompC*^{3}, and *nompC*^{4} mutants and determined their nucleotide sequences. All four alleles have single base changes that result in either nonsense or missense mutations. *nompC*^{1}, *nompC*^{2}, and

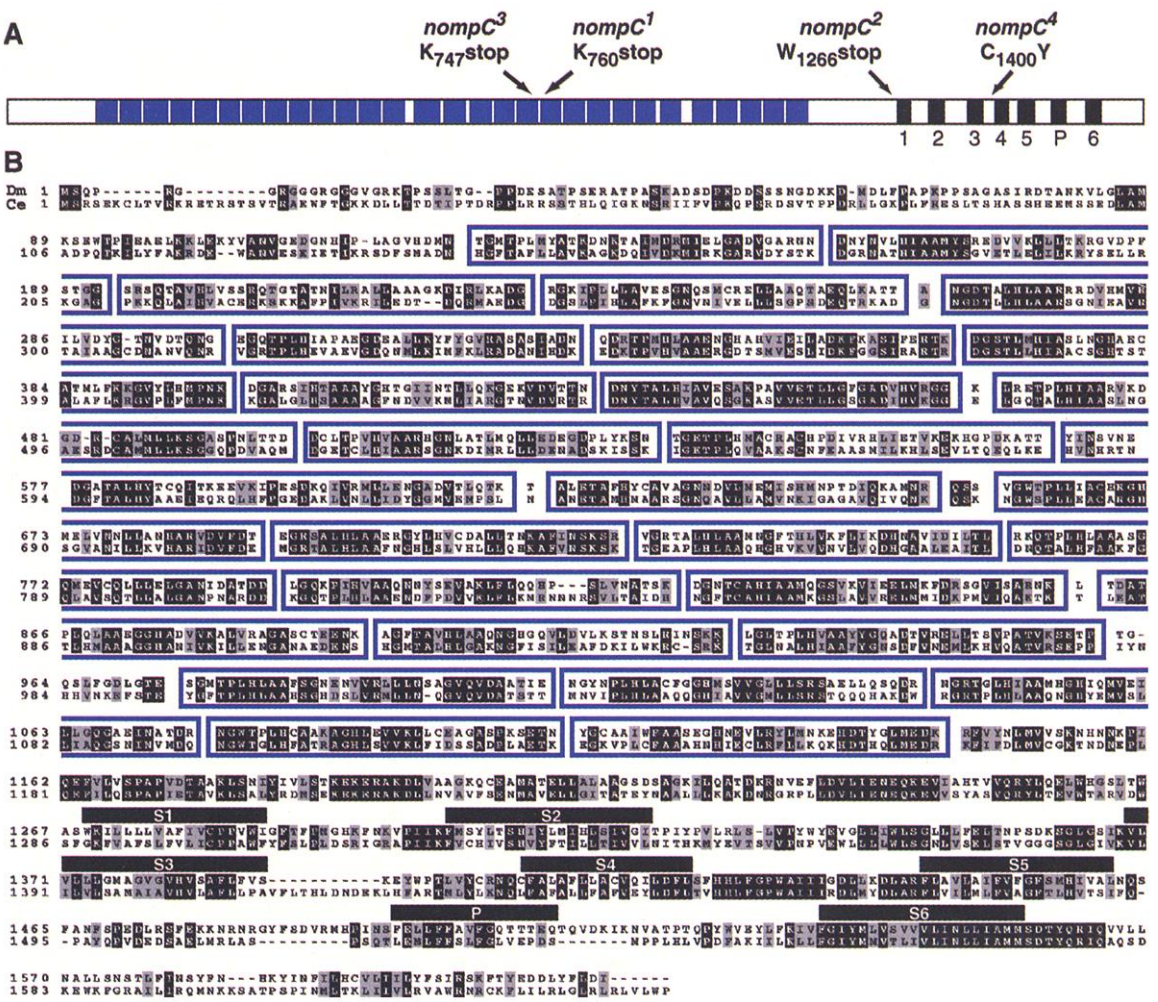

Fig. 6. *nompC* encodes a new ion channel. (**A**) NOMPC is a 1619–amino acid protein (*26*) with 29 ANK repeats (blue boxes) and six predicted transmembrane domains (black boxes); P refers to putative pore region. The four *nompC* mutations are indicated above the protein feature map. (**B**) Alignment of *D. melanogaster* and *C. elegans* NOMPC proteins. The two sequences display 41% identity (black shading) and 58% similarity (gray shading). The 29 ANK repeats are indicated by blue boxes; the six predicted transmembrane domains (S1 through S6) are indicated by black bars above the sequence. On the basis of similarity to other ion channels, a proposed pore region (P) was assigned between S5 and S6.

nompC[3] each have nucleotide changes that introduce premature termination codons; in contrast, *nompC*[4] has an A → T change at residue 4820 that results in a C → Y change at amino acid residue 1400 (*26*) (Figs. 5C and 6A).

A search of protein and nucleotide databases revealed that the NOMPC gene encodes a previously unidentified ion channel with an exceptional feature: the 1150 NH_2-terminal amino acid residues consist of 29 ankyrin (ANK) repeats (Fig. 6, A and B). The remaining 469 residues share low but significant sequence similarity with ion channels of the TRP family (*27*). A search of the *C. elegans* (Ce) database identified a homologous ion channel, Ce-NOMPC, that shares ~40% amino acid identity with NOMPC (*24*). The homology extends throughout the entire molecule, including the six transmembrane segments and the presence of 29 ANK repeats (Fig. 6B). ANK repeats are 33-residue motifs that mediate specific protein-protein interactions with a diverse repertoire of macromolecular targets (*28*). Although we do not know the function of the ANK repeats in NOMPC, it is notable that ANK repeats are particularly prominent in the assembly of macromolecular complexes between the plasma membrane and the cytoskeletal network (*29*).

TRPs are a diverse family of cation channels found in both vertebrates and invertebrates and are implicated in calcium signaling (*30*), pain transduction (*31*), and chemosensory transduction (*14*). In all, pairwise comparison between the channel domains of NOMPC and the various TRP family members revealed ~20% identity (~40% similarity), establishing NOMPC as a new distant member of this channel family (*27*).

NOMPC is expressed in mechanosensory organs. To examine the expression pattern of the *nompC* transcript, we performed RNA in situ hybridizations to tissue sections of late-stage pupae (*25*). We found that NOMPC is selectively expressed in ciliated mechanosensory organs, including microchaetes (Fig. 7A), macrochaetes (Fig. 7B), and bristles on the fly's proboscis (Fig. 7C). Control hybridizations with sense probes produced no specific signals in any of these cells (*32*). Given the strong uncoordinated phenotype of *nompC* mutants, we reasoned that *nompC* should also be required in proprioceptive organs, which include the ciliated chordotonal neurons. Indeed, NOMPC is expressed in chordotonal organs of the halteres (Fig. 7D), as well as in the leg joints and Johnston's organ (*32*). The expression profile of *nompC* in mechanoreceptive bristles and chordotonal organs accords with the physiological (loss of MRC) and behavioral (uncoordination) phenotypes of *nompC* mutants and supports NOMPC as a mechanosensory transduction channel.

We wondered why Ce-NOMPC was not isolated in the various screens for *C. elegans* touch-insensitive mutants. As it turns out, body-touch sensitivity in *C. elegans* is mediated by nonciliated touch cells. To determine the expression profile of the *C. elegans* *nompC* gene, we fused 4.5 kb of upstream sequences and the first four ANK repeats of Ce-NOMPC to a green fluorescent protein (GFP) reporter (*24*). The construct was injected into worms, and the transformed progeny was inspected for GFP expression. Multiple transformants were examined, and in all cases, fluorescent signals were observed in CEPV, CEPD, and ADE neurons (Fig. 7, E through G). These mechanosensory neurons have ciliated dendrites and may be the functional equivalent of the fly ciliated mechanosensory neurons (*33, 34*). Notably, the *C. elegans* NOMPC-GFP fusion localized to the sensory dendrites, the proposed site of mech-

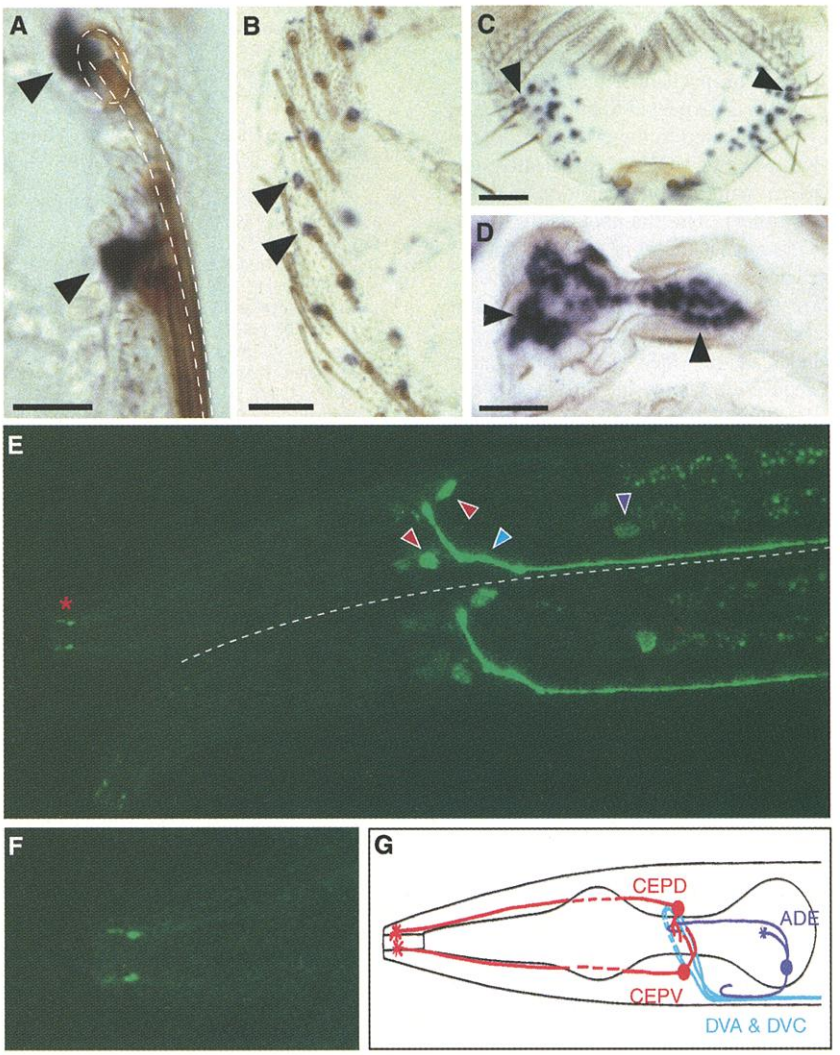

Fig. 7. *nompC* is specifically expressed in mechanosensory organs. Tissue sections (30 μm) of late-stage pupae were hybridized with digoxigenin-labeled *nompC* antisense probes. *nompC* is selectively expressed in mechanosensory organs including (**A**) macrochaetes, (**B**) microchaetes, (**C**) sensory bristles on the proboscis, and (**D**) proprioceptive chordotonal organs of halteres. Each sensillum on the fly's proboscis contains two to four chemosensory neurons and a single mechanosensory neuron. Arrows indicate labeled cells, and dashed lines in (A) delineate the bristle shaft and socket. Scale bar in (A) represents 25 μm; scale bars in (B) through (D) represent 50 μm. (**E**) A 6.2-kb genomic fragment containing 4.5 kb of upstream sequences and exons 1 through 3 (ANK repeats 1 through 4) of Ce-NOMPC was fused in-frame to GFP (*14*). Shown is a lateral view of the anterior region of two worms in confocal fluorescence microscopy. Ce-NOMPC::GFP expression was observed in a subset of ciliated mechanosensory neurons: ADE (purple arrow), CEPD and CEPV (red arrows), as well as interneurons DVA and DVC (blue arrow). Neurons were identified by position and morphology with Nomarski microscopy (*40*). With the exception of DVA and DVC, all neurons are bilaterally symmetric, and only those on the left side are visible in this focal plane. Anterior is to the left and dorsal is up; dotted line denotes the boundary between the two worms. (**F**) Higher power image of the region indicated by the red asterisk in (B). Ce-NOMPC::GFP was targeted to the sensory cilia of CEPV and CEPD neurons. (**G**) The diagram shows the positions of neuronal cell bodies and projections; the soma of DVA and DVC are in the tail of the worm and are not depicted.

anosensory transduction in these cells (Fig. 7F).

Concluding remarks. Several lines of evidence support NOMPC's role as a mechanosensory transduction channel. First, at the primary sequence level, NOMPC has similarity to bona fide ion channels. Second, loss-of-function mutations in *nompC* virtually eliminate mechanoreceptor responses, and a single point mutation in the channel alters the behavior of the transduction currents. Third, *nompC* is selectively expressed in mechanosensory organs in *Drosophila*. Furthermore, the *C. elegans* homolog localizes to the presumed site of mechanoelectrical transduction. Last, it is expected that transduction channels are tethered to the cytoskeleton; the 29 ANK repeats of NOMPC are ideally suited to interact with the cytoskeleton and transduction partners. This number of ANK repeats is the largest found in any protein.

Like many other ion channels, NOMPC may form a multimeric channel. If individual subunits are linked to the cytoskeleton or the extracellular matrix, then mechanical gating can be reduced to simply altering tension between the NOMPC subunits. In this model, deflection of the bristle deforms the dendritic tip (Fig. 1A), which shifts the position of the channel's anchor points in relation to each other. The resulting tension across the molecule would trigger a conformational change that opens the molecular gate of the NOMPC transduction channel. We anticipate at least two ways that NOMPC may be integrated into the transduction apparatus. In one, NOMPC could be attached on both sides of the plasma membrane: to the cytoskeleton through the extensive ANK repeats and to the extracellular matrix through a different channel subunit or additional binding proteins. Alternatively, NOMPC need not be linked to the extracellular matrix. Instead, the cytoplasmic anchoring of individual subunits or membrane stress (*35*) may provide sufficient tension to modulate the molecular gate.

Although null mutations in *nompC* virtually eliminated the transduction current, there is a tiny mechanically gated residual response in these mutants (Fig. 4A), suggesting the presence of an additional mechanically gated channel. In view of NOMPC's similarity to TRP channels, which together with the TRP-like ion channel generate the light-activated conductance in *Drosophila* photoreceptors (*30*), NOMPC might participate in a transduction current with another channel (*36*).

Are there vertebrate NOMPC channels? The transduction physiology of *Drosophila* mechanoreceptor bristles mirrors that of vertebrate hair cells, including the presence of a high-K^+, low-Ca^{2+} receptor endolymph, directional sensitivity, microsecond latencies, sensitivity to displacements of molecular dimensions, and similar adaptation profiles. In addition, the development of vertebrate hair cells and *Drosophila* mechanoreceptor organs employ homologous cell-signaling molecules, insinuating common downstream targets (*37, 38*). It will be of great interest to determine if there are NOMPC homologs in vertebrates and whether they underlie any sensory deafness or disequilibrium disorders.

References and Notes

1. D. P. Corey and A. J. Hudspeth, *Biophys. J.* **26**, 499 (1979).
2. J. Howard and A. J. Hudspeth, *Neuron* **1**, 189 (1988).
3. V. S. Markin and A. J. Hudspeth, *Annu. Rev. Biophys. Biomol. Struct.* **24**, 59 (1995).
4. A. J. Hudspeth, *Nature* **341**, 397 (1989).
5. Y. Saimi and C. Kung, *Annu. Rev. Genet.* **21**, 47 (1987).
6. M. Chalfie and J. Sulston, *Dev. Biol.* **82**, 358 (1981).
7. M. Kernan, D. Cowan, C. Zuker, *Neuron* **12**, 1195 (1994).
8. D. F. Eberl, G. M. Duyk, N. Perrimon, *Proc. Natl. Acad. Sci. U.S.A.* **94**, 14837 (1997).
9. T. T. Whitfield *et al.*, *Development* **123**, 241 (1996).
10. D. M. Fekete, *Trends Neurosci.* **22**, 263 (1999).
11. M. Chalfie and M. Au, *Science* **243**, 1027 (1989).
12. J. García-Añoveros and D. P. Corey, *Annu. Rev. Neurosci.* **20**, 567 (1997).
13. I. Mano and M. Driscoll, *Bioessays* **21**, 568 (1999).
14. H. A. Colbert, T. L. Smith, C. I. Bargmann, *J. Neurosci.* **17**, 8259 (1997).
15. M. Kernan and C. Zuker, *Curr. Opin. Neurobiol.* **5**, 443 (1995).
16. U. Thurm, *Cold Spring Harbor Symp. Quant. Biol.* **30**, 75 (1965).
17. G. Corfas and Y. Dudai, *J. Neurosci.* **10**, 491 (1990).
18. Unless indicated otherwise, all wild-type recordings were made from the Canton S strain. Other strains and stocks were obtained from either the Bloomington *Drosophila* Stock Center, J. Szidonya, or L. Lorenz or were generated in our laboratory. Mechanosensory mutants were prepared for recording, and pipette solutions were as described (*7*). In this preparation, we clamped the transepithelial potential (TEP) at +40 mV, the average TEP for wild-type bristles. The recording configuration consisted of two electrodes: a reference electrode placed in the thorax of the fly and a recording/stimulation electrode slipped over the end of a cut bristle, thus making a circuit across the sensory epithelium through the hollow bristle. Voltage and current responses were measured through a modified headstage with a voltage-clamp amplifier (AxoPatch 1-D, Axon Instruments, Foster City, CA) in either current- or voltage-clamp mode with series resistance and capacitance compensation. Responses were low-pass filtered at half-power frequencies of 100 to 10,000 Hz before sampling at intervals of 6 to 2000 μs. After subtraction of 4-mV liquid junction potential, the resting potential across the mechanosensory epithelium was, on average, 41 mV. Movements of the recording electrode were driven by a piezoelectrical stage (PZS-100HS, Burleigh Instruments, Fishers, NY). To eliminate mechanical resonance of the pipette, input signals driving the piezoelectrical device were low-pass filtered at a half-power frequency of 100 Hz (10 kHz for Fig. 2C; 1 kHz for action potentials) with an eight-pole Bessel filter (Model 3282, Krohn-Hite, Avon, MA). In Figs. 1 through 7, the stimulus trace represents the driving voltage to the piezoelectric device. Displacements of the stimulus probe were calibrated with an etched micrometer grid. Bristles were displaced over a range of ±35 μm. The bristle position faithfully followed that of the stimulating electrode.
19. T. A. Keil, *Microsc. Res. Tech.* **39**, 506 (1997).
20. A. C. Crawford, M. G. Evans, R. Fettiplace, *J. Physiol. (London)* **419**, 405 (1989).
21. R. G. Walker, T. A. Keil, C. S. Zuker, unpublished observations.
22. R. A. Eatock, D. P. Corey, A. J. Hudspeth, *J. Neurosci.* **7**, 2821 (1987).
23. M. Kernan, D. Cowan, C. Zuker, unpublished results.
24. *nompC* corresponds to *l(2)25Dc*. DNA cloning, sequencing, characterization of mutant alleles, and *Drosophila melanogaster* (Dm) transformations were performed as described by L. Wu, B. Niemeyer, N. Colley, M. Socolich, C. S. Zuker, *Nature* **373**, 216 (1995). *nompC* cDNAs were identified with a 0.7-kb probe from exon 12 to screen an antennal cDNA library. *Ce-nompC* gene structure and protein sequence were predicted by the program FGENESH and modified by the deletion of a 70–amino acid sequence (the end of exon 8 and the beginning of exon 9), which introduced a hydrophobic segment in the midst of an ANK repeat that was inconsistent with Dm-NOMPC's structure. Extension of exon 19 by 54 base pairs produced 18 additional amino acid residues with homology to Dm-NOMPC followed by three stop codons. A translational fusion of Ce-NOMPC and GFP was constructed with a GFP expression vector, pPD95.81. A 6.2-kb *Ce-nompC* sequence was amplified by long-range PCR from genomic DNA (wild-type strain N2) with a primer 4.5 kb upstream of the presumptive initiator methionine and a primer corresponding to the end of the third exon. Clones were sequenced at the site of insertion to ensure proper orientation of the insert within the vector. Germ line transformation was performed as described (*15*). Worms from six independent transgenic lines were viewed by fluorescence microscopy; cell position and morphology were used to identify neurons.
25. L. B. Vosshall, H. Amrein, P. S. Morozov, A. Rzhetsky, R. Axel, *Cell* **96**, 725 (1999).
26. Single-letter abbreviations for the amino acid residues are as follows: A, Ala; C, Cys; D, Asp; E, Glu; F, Phe; G, Gly; H, His; I, Ile; K, Lys; L, Leu; M, Met; N, Asn; P, Pro; Q, Gln; R, Arg; S, Ser; T, Thr; V, Val; W, Trp; and Y, Tyr.
27. See Web fig. 1, available at www.sciencemag.org/feature/data/1048845.shl.
28. S. G. Sedgwick and S. J. Smerdon, *Trends Biochem. Sci.* **24**, 311 (1999).
29. E. J. Luna, *Curr. Opin. Cell Biol.* **3**, 120 (1991).
30. K. Scott and C. Zuker, *Curr. Opin. Neurobiol.* **8**, 383 (1998).
31. M. J. Caterina *et al.*, *Nature* **389**, 816 (1997).
32. R. G. Walker and C. S. Zuker, unpublished observations.
33. L. A. Perkins, E. M. Hedgecock, J. N. Thomson, J. G. Culotti, *Dev. Biol.* **117**, 456 (1986).
34. E. R. Sawin, thesis, Massachusetts Institute of Technology (1996).
35. M. Kanzaki *et al.*, *Science* **285**, 882 (1999).
36. Using a variety of screening strategies, we searched genomic and cDNA libraries for homologs of NOMPC but did not identify additional related molecules. Searches of the >90%-complete *Drosophila* genomic sequence also failed to identify NOMPC homologs. Additional related channels, however, may reside in the unsequenced gaps, or a different type of channel may mediate the current remaining in *nompC* mutants.
37. A. Morrison, C. Hodgetts, A. Gossler, M. Hrabe de Angelis, J. Lewis, *Mech. Dev.* **84**, 169 (1999).
38. N. A. Bermingham *et al.*, *Science* **284**, 1837 (1999).
39. H. George and R. Terracol, *Genetics* **146**, 1345 (1997).
40. J. G. White, E. Southgate, J. N. Thomson, S. Brenner, *Philos. Trans. R. Soc. London Ser. B* **314**, 1 (1986).

41. We acknowledge M. Kernan for introducing us to *Drosophila* mechanotransduction and for his pioneering and inspiring genetic studies, including the isolation of *nomp* mutants. We thank K. Jalink for assistance in constructing the voltage-clamp apparatus, J. Szidonya and L. Lorenz for providing fly stocks, T. Keil for electron microscopy, R. Terracol for sharing her chromosomal walk, and L. Vosshall for providing an antennal cDNA library. We also thank K. Scott for her invaluable assistance with in situ hybridizations and C. Bargmann and D. Tobin for their hospitality, expertise, and advice with the *C. elegans* experiments. S. Emr, P. Gillespie, K. Scott, R. Tsien, and members of our laboratory kindly proffered constructive comments on the manuscript. R.G.W. is a postdoctoral fellow of the American Cancer Society (PF-4470); A.T.W. was supported by NIH training grant 5T32GM08107. C.S.Z. is an Investigator of the Howard Hughes Medical Institute.

21 January 2000; accepted 25 February 2000